

Modeling the uncertainty on the covariance matrix for probabilistic forecast reconciliation

Chiara Carrara^{a,*}, Lorenzo Zambon^b, Dario Azzimonti^b, Giorgio Corani^b

^a*University of Pavia*

^b*SUPSI, Istituto Dalle Molle di Studi sull'Intelligenza Artificiale (IDSIA)*

Abstract

In forecast reconciliation, the covariance matrix of the base forecasts errors plays a crucial role. Typically, this matrix is estimated, and then treated as known. In contrast, we propose a Bayesian reconciliation model that explicitly accounts for the uncertainty in the covariance matrix. We choose an Inverse-Wishart prior, which leads to a multivariate-t reconciled predictive distribution and allows a completely analytical derivation. Empirical experiments demonstrate that this approach improves the accuracy of the prediction intervals with respect to MinT, leading to more reliable probabilistic forecasts.

Keywords: Probabilistic forecast reconciliation, Covariance matrix uncertainty, Bayesian modeling

1. Introduction

Hierarchical forecasts are usually obtained by producing incoherent base forecasts and then reconciling them. Theoretical results, such as the optimality of MinT (Wickramasuriya, Athanasopoulos & Hyndman, 2019), assume the covariance matrix of the errors of the base forecasts to be known. In practice, the covariance matrix is instead estimated from the in-sample residuals. An inaccurate estimation of the covariance matrix can largely affect the accuracy of the reconciled forecasts (Pritularga, Svetunkov & Kourentzes, 2021). However, the current reconciliation algorithms (Wickramasuriya et al., 2019; Corani, Azzimonti, Augusto & Zaffalon, 2020; Wickramasuriya, 2024; Yang, Athanasopoulos, Hyndman & Panagiotelis, 2024; Girolimetto, Athanasopoulos, Di Fonzo & Hyndman, 2024) do not consider the uncertainty of the covariance matrix; this can lead to overconfident predictions. Generally they rely on the shrinkage estimator (Schäfer & Strimmer, 2005) of the covariance matrix, which offers improved accuracy over the sample covariance but remains a point estimate. While some efforts have been made to enhance this estimate (Wickramasuriya, 2017; Carrara, Zambon, Azzimonti & Corani, 2025), they either offer limited improvements or incur significant computational cost.

Bayesian inference propagates the uncertainty about the parameters to the predictive distribution (Gelman, Carlin, Stern, Dunson, Vehtari & Rubin, 2013, Chap 1.3), which generally results in a more accurate assessment of the uncertainty. We thus propose a Bayesian reconciliation approach which accounts for the uncertainty of the covariance matrix \mathbf{W} . We call it *t-Rec*, since the reconciled distribution is multivariate t. In order to set the prior distribution on \mathbf{W} we consider as prior information the covariance of in-sample residuals of simple forecasting methods such as naive and seasonal naive. The posterior distribution of \mathbf{W} is obtained by updating the prior with the evidence constituted by the covariance of the residuals of the forecast method actually used to generate the base forecasts (ets, auto.arima, etc). We assume that the base forecast residuals are conditionally multivariate normal given \mathbf{W} . Marginalizing over \mathbf{W} , the predictive distribution of the base forecast is a multivariate t-distribution rather than a Gaussian. This distribution is however incoherent and needs to be reconciled.

We adopt reconciliation via conditioning (Corani et al., 2020; Zambon, Azzimonti & Corani, 2024b). We perform the conditioning in closed form thanks to the closure of the multivariate t under affine transforma-

*Corresponding author

Email address: chiara.carrara03@universitadipavia.it (Chiara Carrara)

tions and conditioning. Thus we analytically obtain the reconciled distribution that remains a multivariate t-distribution.

On the point forecasts *t-Rec* has almost the same performance of probabilistic Gaussian reconciliation (Zambon et al., 2024b; Wickramasuriya, 2024); its main advantage is the improvement of the prediction intervals, thanks to heavier tails of the predictive distribution. Indeed, *t-Rec* manages the prediction intervals in a more sophisticated way than Gaussian reconciliation, which always reduce (Zambon, Agosto, Giudici & Corani, 2024a) the variance and thus the length of the prediction intervals compared to the base forecasts. Instead, the prediction intervals of *t-Rec* can also be larger than those of the base forecasts; this happens in case of large incoherence. *t-Rec* implies a only small computation overhead compared to probabilistic Gaussian reconciliation, since its computations are mostly analytical.

The paper is structured as follow: in Sect. 2 we introduce the notation, we recall the concepts of probabilistic reconciliation and MinT reconciliation; in Sect. 3 we analytically derive *t-Rec* and we discuss its specifications; in Sect. 4 we show how the model behaves on a minimal hierarchy; in Sect. 5 we report empirical results on real datasets; in Sect. 6 we present our conclusions.

2. Probabilistic reconciliation

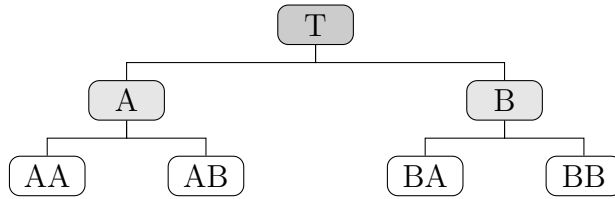


Figure 1: Hierarchy with 4 bottom and 3 upper time series.

Hierarchical time series are collections of time series formed via aggregation, which satisfy some summing constraints. Fig. 1 can represent, for example, the total visitors of a country (T), disaggregated by zones (A, B) and regions (AA, AB, BA, BB), so that:

$$T = A + B, \quad A = AA + AB, \quad B = BA + BB.$$

At any time t , the hierarchical constraints between time series are given by:

$$\mathbf{u}_t = \mathbf{Ab}_t, \quad (1)$$

where $\mathbf{A} \in \mathbb{R}^{n_u \times n_b}$ is the *aggregation matrix*, which is made of 0 and 1 and specifies how the *bottom* time series $\mathbf{b}_t \in \mathbb{R}^{n_b}$ aggregate to the *upper* time series $\mathbf{u}_t \in \mathbb{R}^{n_u}$. The *summing matrix* $\mathbf{S} \in \mathbb{R}^{n_u \times n_b}$, defined as:

$$\mathbf{S} = \begin{bmatrix} \mathbf{A} \\ \mathbf{I}_{n_b \times n_b} \end{bmatrix},$$

encodes the hierarchy via $\mathbf{y}_t = \mathbf{Sb}_t$, where $\mathbf{y}_t = [\mathbf{u}_t^T, \mathbf{b}_t^T]^T \in \mathbb{R}^n$.

We adopt the formulation based on the summation matrix, although all the reasoning extends to the more general linearly constrained time series framework introduced in Girolimetto & Fonzo (2024).

We consider probabilistic forecasts in the form of a joint predictive distribution $\hat{\pi}$ over \mathbb{R}^n . The forecast distribution $\hat{\pi}$ should be *coherent*, i.e., it should give positive probability only to regions of points that satisfy the hierarchical constraints. Hence, the support of $\hat{\pi}$ should lie on the *coherent subspace* \mathcal{S} , defined as $\mathcal{S} := \{\mathbf{y} \in \mathbb{R}^n \text{ such that } \mathbf{y} = \mathbf{Sb}\}$, so that any sample from $\hat{\pi}$ satisfies the hierarchical constraints. The goal of probabilistic reconciliation is to find a coherent reconciled forecast distribution $\tilde{\pi}$. For a more detailed discussion on probabilistic reconciliation, we refer to Panagiotelis, Gamakumara, Athanasopoulos & Hyndman (2023); Zambon et al. (2024b).

MinT reconciliation. The Minimum Trace (MinT) reconciliation method was initially introduced for the reconciliation of point forecasts by Wickramasuriya et al. (2019). Given the h -step ahead base point forecasts $\hat{\mathbf{y}}_{t+h|t}$, computed at time t for time $t+h$, the reconciled point forecasts $\tilde{\mathbf{y}}_{t+h|t}$ are obtained by projecting $\hat{\mathbf{y}}_{t+h|t}$ on the coherent subspace \mathcal{S} :

$$\tilde{\mathbf{y}}_{t+h|t} = \mathbf{S}\mathbf{P}_h\hat{\mathbf{y}}_{t+h|t}, \quad (2)$$

where $\mathbf{P}_h = (\mathbf{S}^T \mathbf{W}_h^{-1} \mathbf{S})^{-1} \mathbf{S}^T \mathbf{W}_h^{-1}$, and \mathbf{W}_h is the covariance matrix of the h -step ahead base forecast errors. Assuming that the base forecasts $\hat{\mathbf{y}}_{t+h|t}$ are unbiased and that the matrix \mathbf{W}_h is known, the reconciled point forecasts $\tilde{\mathbf{y}}_{t+h|t}$ are optimal in terms of the Mean Squared Error (MSE).

MinT was later extended to the probabilistic case by projecting on \mathcal{S} the entire forecast distribution $\tilde{\pi}$ (Panagiotelis et al., 2023). If the joint base forecast distribution is Gaussian, i.e., $\tilde{\pi} = \text{MVN}(\hat{\mathbf{y}}_{t+h|t}, \mathbf{W}_h)$, the reconciled distribution is also Gaussian:

$$\tilde{\pi} = \text{MVN}(\tilde{\mathbf{y}}_{t+h|t}, \tilde{\mathbf{W}}_h),$$

where $\tilde{\mathbf{y}}_{t+h|t}$ is given by Eq. (2) and $\tilde{\mathbf{W}}_h = \mathbf{S}\mathbf{P}_h\mathbf{W}_h\mathbf{P}_h^T\mathbf{S}^T$. In the Gaussian case, $\tilde{\pi}$ is optimal with respect to the log-score (Wickramasuriya, 2024).

Probabilistic reconciliation via conditioning. The reconciled distribution can be obtained by conditioning the joint forecast distribution on the hierarchy constraints (Corani et al., 2020; Zambon et al., 2024b). Given $\hat{\mathbf{Y}} = [\hat{\mathbf{U}}^T, \hat{\mathbf{B}}^T]^T$, a random vector distributed as the h -step ahead base forecast distribution $\hat{\pi}$; the reconciled distribution of the bottom series is given by

$$\tilde{\mathbf{B}} \sim \hat{\mathbf{B}} \mid (\hat{\mathbf{U}} - \mathbf{A}\hat{\mathbf{B}} = 0),$$

and can be extended to the entire hierarchy by pre-multiplying by \mathbf{S} (Zambon et al., 2024b). If the base forecast distribution is jointly Gaussian, the solution of reconciliation via conditioning coincides with MinT (Corani et al., 2020; Zambon, Azzimonti, Rubattu & Corani, 2024c).

Estimation of \mathbf{W}_1 . For $h = 1$, \mathbf{W}_1 is typically estimated as the covariance matrix of the in-sample residuals. Empirically, the most effective choice (Wickramasuriya et al., 2019; Panagiotelis, Athanasopoulos, Gamakumara & Hyndman, 2021; Di Fonzo & Girolimetto, 2024) appears to be the shrinkage estimator (Schäfer & Strimmer, 2005), defined as

$$\hat{\Sigma}_{\text{shrink}} = (1 - \lambda_{\text{shrink}})\hat{\mathbf{W}} + \lambda_{\text{shrink}}\hat{\mathbf{D}}, \quad (3)$$

where $\hat{\mathbf{W}}$ is the sample covariance matrix, $\hat{\mathbf{D}}$ is the diagonal matrix of the sample variances, and $\lambda_{\text{shrink}} \in [0, 1]$ is the optimal shrinkage parameter. We denote the MinT reconciliation method with the shrinkage estimator by *MinT*.

Estimation of \mathbf{W}_h . There is no standard method for estimating \mathbf{W}_h for $h > 1$. Wickramasuriya et al. (2019) assume $\mathbf{W}_h = k_h \mathbf{W}_1$ for some constant k_h , which does not need to be estimated to compute the reconciled point forecast $\tilde{\mathbf{y}}_{t+h|t}$. Yet, in a probabilistic framework, k_h is needed to compute the reconciled variance; some heuristic strategies have been proposed by Corani et al. (2020). Alternative approaches are given by Girolimetto et al. (2024), where \mathbf{W}_h is estimated using multi-step residuals. Our method can be applied with any choice of \mathbf{W}_h ; in our experiments, we only consider the case $h = 1$. From now on, we drop the h subscript for ease of notation.

3. Probabilistic reconciliation with uncertain \mathbf{W}

Prior of \mathbf{W} . We adopt an Inverse-Wishart (IW) prior distribution for \mathbf{W} . Hence, we set

$$\mathbf{W} \sim \text{IW}(\mathbf{\Psi}_0, \nu_0), \quad (4)$$

where $\mathbf{\Psi}_0 \in \mathbb{R}^{n \times n}$ is the scale parameter and $\nu_0 \in \mathbb{R}$ is the degree of freedom. The Inverse-Wishart is a distribution defined on the space of positive-definite matrices, with density

$$\text{IW}(\mathbf{W}; \mathbf{\Psi}_0, \nu_0) = \frac{|\mathbf{\Psi}_0|^{\frac{\nu_0}{2}}}{2^{\frac{n\nu_0}{2}} \Gamma_n(\frac{\nu_0}{2})} |\mathbf{W}|^{-\frac{\nu_0+n+1}{2}} \exp\left(-\frac{\text{tr}(\mathbf{\Psi}_0 \mathbf{W}^{-1})}{2}\right),$$

where $|\cdot|$ denotes the determinant, tr the trace, and Γ_n the multivariate gamma function (Gupta & Nagar, 2018).

Likelihood. As in Corani et al. (2020); Wickramasuriya (2024), we assume that, conditionally on \mathbf{W} , the base predictive distribution is Gaussian with covariance matrix \mathbf{W} , and that the base forecasts are unbiased. The in-sample residuals $\mathbf{r}_1, \dots, \mathbf{r}_T$, defined as $\mathbf{r}_j = \hat{\mathbf{y}}_j - \mathbf{y}_j$ for $j = 1, \dots, T$, are thus an IID sample from a multivariate Gaussian with zero mean and covariance matrix \mathbf{W} :

$$\mathbf{r}_1, \dots, \mathbf{r}_T \mid \mathbf{W} \stackrel{\text{IID}}{\sim} \text{MVN}(\mathbf{0}, \mathbf{W}). \quad (5)$$

Posterior of \mathbf{W} . The posterior distribution of \mathbf{W} , since the IW is conjugate for the multivariate Gaussian likelihood (Gelman et al., 2013, Ch. 3.6), is still Inverse-Wishart:

$$\pi(\mathbf{W} \mid \mathbf{R}) = \text{IW}(\mathbf{W}; \Psi', \nu'), \quad (6)$$

with parameters $\nu' = \nu_0 + T$ and $\Psi' = \Psi_0 + \mathbf{R}\mathbf{R}^T$, where $\mathbf{R} := [\mathbf{r}_1 \dots \mathbf{r}_T] \in \mathbb{R}^{n \times T}$ is the matrix of the in-sample residuals.

Multivariate t base predictive distribution. We obtain the incoherent posterior predictive distribution of the base forecasts, by marginalizing out \mathbf{W} ; it is a multivariate t-distribution (Gelman et al., 2013, Ch. 3.6):

$$\begin{aligned} \hat{\pi}(\mathbf{y} \mid \mathbf{R}) &= \int \hat{\pi}(\mathbf{y}, \mathbf{W} \mid \mathbf{R}) d\mathbf{W} \\ &= \int \hat{\pi}(\mathbf{y} \mid \mathbf{W}) \pi(\mathbf{W} \mid \mathbf{R}) d\mathbf{W} \\ &= \int \text{MVN}(\mathbf{y}; \hat{\mathbf{y}}, \mathbf{W}) \text{IW}(\mathbf{W}; \Psi', \nu') d\mathbf{W} \\ &= \text{mt}\left(\mathbf{y}; \hat{\mathbf{y}}, \frac{1}{\nu' - n + 1} \Psi', \nu' - n + 1\right). \end{aligned} \quad (7)$$

Reconciliation. The multivariate t-distribution is closed under affine transformations and conditioning (Kotz & Nadarajah, 2004). Hence, we obtain analytically the reconciled distribution via conditioning, as stated the following theorem, which we prove in Appendix A.

Theorem 1. *Given a hierarchy specified by Eq. (1), and under the model of Eq. (5) and Eq. (4), the reconciled distribution via conditioning of the bottom time series is a multivariate t-distribution:*

$$\tilde{\mathbf{B}} \sim \text{mt}\left(\tilde{\mathbf{b}}, \tilde{\Sigma}_B, \tilde{\nu}\right), \quad (8)$$

where

$$\tilde{\mathbf{b}} = \hat{\mathbf{b}} + \left(\Psi'_{UB}^T - \Psi'_B \mathbf{A}^T\right) \mathbf{Q}^{-1}(\mathbf{A}\hat{\mathbf{b}} - \hat{\mathbf{u}}), \quad (9)$$

$$\tilde{\Sigma}_B = C \left[\Psi'_B - \left(\Psi'_{UB}^T - \Psi'_B \mathbf{A}^T\right) \mathbf{Q}^{-1} \left(\Psi'_{UB}^T - \Psi'_B \mathbf{A}^T\right)^T \right], \quad (10)$$

$$\tilde{\nu} = \nu' - n_b + 1, \quad (11)$$

and

$$\begin{aligned} C &= \frac{1 + (\mathbf{A}\hat{\mathbf{b}} - \hat{\mathbf{u}})^T \mathbf{Q}^{-1}(\mathbf{A}\hat{\mathbf{b}} - \hat{\mathbf{u}})}{\tilde{\nu}}, \\ \mathbf{Q} &= \Psi'_U - \Psi'_{UB} \mathbf{A}^T - \mathbf{A} \Psi'_{UB}^T + \mathbf{A} \Psi'_B \mathbf{A}^T. \end{aligned}$$

Theorem 1 provides the reconciled distribution for the bottom-level series. The reconciled distribution for the entire hierarchy, obtained by pre-multiplying by the summing matrix \mathbf{S} , is a multivariate t with mean $\tilde{\mathbf{y}} = \mathbf{S}\tilde{\mathbf{b}}$, scale matrix $\mathbf{S}\tilde{\Sigma}_B\mathbf{S}^T$, and degrees of freedom $\tilde{\nu}$.

3.1. Parameters of the prior distribution

We now show how to choose the scale matrix Ψ_0 and the degree of freedom ν_0 of the Inverse-Wishart prior.

Scale matrix. $\Psi_0 \in \mathbb{R}^{n \times n}$ is a positive definite matrix, defined to be proportional to the expected value Ψ of the distribution via $\Psi_0 = (\nu_0 - n - 1)\Psi$. We set Ψ as the shrinkage estimate of the covariance matrix of the residuals from a baseline method. For each time series, the baseline method is selected between the naive and the seasonal naive approach based on the outcome of the KPSS seasonality test, as implemented in the `forecast` package (Hyndman & Khandakar, 2008).

We empirically show in Appendix C that using a diagonal scale matrix prior yields lower performances; this highlights that incorporating the full covariance structure is beneficial for improving reconciliation accuracy.

Degree of freedom. We set $\nu_o \in \mathbb{R}$, maximizing the model's out-of-sample predictive accuracy by using Bayesian leave-one-out (LOO) cross-validation (Vehtari, Gelman & Gabry, 2017):

$$\begin{aligned} \nu_o &:= \arg \max_{\nu \in [n+2, 5n]} \log \left(\prod_{i=1}^T \pi(\mathbf{r}_i \mid \mathbf{R}_{-i}) \right) \\ &= \arg \max_{\nu \in [n+2, 5n]} \sum_{i=1}^T \log \left(\text{mt} \left(\mathbf{r}_i; 0, \frac{1}{\nu + T - n} (\Psi_0 + \mathbf{R}_{-i} \mathbf{R}_{-i}^T), \nu + T - n \right) \right), \end{aligned} \quad (12)$$

where $\mathbf{R}_{-i} \in \mathbb{R}^{n \times (T-1)}$ is the matrix of the in-sample residuals without the column \mathbf{r}_i , and $\pi(\mathbf{r}_i \mid \mathbf{R}_{-i})$ is the posterior predictive density of the residuals \mathbf{r}_i , given the observations \mathbf{R}_{-i} . Note that Eq. (12) follows from Eq. (7), with \mathbf{R} replaced by \mathbf{R}_{-i} and T by $T - 1$. We restrict the search for the optimal value of ν_0 to the interval $[n + 2, 5n]$, since the expected value of the IW prior is not defined for $\nu_0 < n + 2$. The upper bound $\nu_0 = 5n$ is sufficiently large such that, in our experiments, the optimal ν_0 is consistently below it.

A naive evaluation of the objective function in Eq. (12) is computationally expensive as it requires the inversion of the T matrices $\Psi_0 + \mathbf{R}_{-i} \mathbf{R}_{-i}^T$, for $i = 1, \dots, T$. However, since these matrices are rank-1 updates of the same matrix: $\Psi_0 + \mathbf{R}_{-i} \mathbf{R}_{-i}^T = \Psi_0 + \mathbf{R} \mathbf{R}^T - \mathbf{r}_i \mathbf{r}_i^T$, we use the Sherman-Morrison formula (Sherman & Morrison, 1950) to obtain

$$(\Psi_0 + \mathbf{R}_{-i} \mathbf{R}_{-i}^T)^{-1} = (\Psi_0 + \mathbf{R} \mathbf{R}^T)^{-1} + \left(1 + \mathbf{r}_i^T (\Psi_0 + \mathbf{R} \mathbf{R}^T)^{-1} \mathbf{r}_i \right)^{-1} (\Psi_0 + \mathbf{R} \mathbf{R}^T)^{-1} \mathbf{r}_i \mathbf{r}_i^T (\Psi_0 + \mathbf{R} \mathbf{R}^T)^{-1}.$$

We thus compute only once the inverse of the matrix $\Psi_0 + \mathbf{R} \mathbf{R}^T$, achieving a significant speed-up. The optimization of ν is performed using the `nloptr` R package (Johnson, 2008). In our experiments, in the worst case scenario ($n = 111$, $T = 60$), the optimization requires less than 0.5 s on a standard laptop.

4. Application to a minimal hierarchy

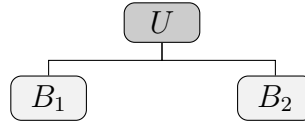


Figure 2: Hierarchy with one upper and two bottom series.

We compare *t-Rec* and *MinT* on the minimal hierarchy of Fig. 2. In this setting the reconciled bottom and upper distribution are:

$$\tilde{\mathbf{B}} \sim \text{mt} \left(\tilde{\mathbf{b}}, \tilde{\Sigma}_B, \tilde{\nu} \right), \quad \tilde{U} \sim t(\tilde{u}, \tilde{\sigma}_u, \tilde{\nu}), \quad (13)$$

where

$$\tilde{\nu} = \nu_0 - 1, \quad \tilde{\mathbf{b}} = \begin{bmatrix} \left(1 - \frac{g_1}{Q}\right)\hat{b}_1 + \frac{g_1}{Q}\left(\hat{u} - \hat{b}_2\right) \\ \left(1 - \frac{g_2}{Q}\right)\hat{b}_2 + \frac{g_2}{Q}\left(\hat{u} - \hat{b}_1\right) \end{bmatrix}, \quad \tilde{u} = \left(1 - \frac{g_u}{Q}\right)\hat{u} + \frac{g_u}{Q}\left(\hat{b}_1 + \hat{b}_2\right), \quad (14)$$

$$\tilde{\Sigma}_B = C \begin{bmatrix} \Psi'_1 - \frac{g_1^2}{Q} & \Psi'_{1,2} - \frac{g_1 g_2}{Q} \\ \Psi'_{1,2} - \frac{g_1 g_2}{Q} & \Psi'_2 - \frac{g_2^2}{Q} \end{bmatrix}, \quad \tilde{\sigma}_u^2 = C \left(\Psi'_u - \frac{g_u^2}{Q} \right), \quad (15)$$

and

$$C = \frac{1}{\tilde{\nu}} \left(1 + \frac{(\hat{b}_1 + \hat{b}_2 - \hat{u})^2}{Q} \right), \quad Q = g_1 + g_2 + g_u, \\ g_1 = (\Psi'_1 + \Psi'_{1,2}) - \Psi'_{u,1}, \quad \Psi_0 = \begin{bmatrix} \Psi'_u & \Psi'_{u,1} & \Psi'_{u,2} \\ \Psi'_{u,1} & \Psi'_1 & \Psi'_{1,2} \\ \Psi'_{u,2} & \Psi'_{1,2} & \Psi'_2 \end{bmatrix}. \\ g_2 = (\Psi'_2 + \Psi'_{1,2}) - \Psi'_{u,2}, \\ g_u = \Psi'_u - \Psi'_{u,1} - \Psi'_{u,2},$$

The reconciled point forecasts (Eq. 14) are a combination of the base point forecasts; for example, the reconciled upper mean \tilde{u} is a convex combination of \hat{u} and $\hat{b}_1 + \hat{b}_2$. This was already observed in the Gaussian case (Hollyman, Petropoulos & Tipping, 2021; Zambon et al., 2024a).

However, there is an important difference in the reconciled prediction intervals. In the Gaussian case, the width of the prediction intervals decreases after reconciliation since the reconciled variance is smaller than the variance of the base forecasts (Zambon et al., 2024a). In contrast, the prediction intervals of *t-Rec* can become wider than those of the base forecasts in case of large incoherence; indeed, the scale parameters in Eq. 15 depend on the incoherence $\mathbf{A}\hat{\mathbf{b}} - \hat{u}$ through the term C .

4.1. Simulations

We compare the prediction intervals of *MinT* and *t-Rec* using simulated time series. We run 1000 simulations, in which we simulate the time series, compute the base forecasts, and reconcile them. As in Wickramasuriya et al. (2019), we simulate the two bottom series with a structural time series model with trend, seasonality and correlated errors. The seasonality is set to 4, and the training length to 12. More details are reported in Appendix B. We obtain the upper series as the sum of the bottom series. We introduce model misspecification by computing the base forecasts with ets model with additive noise from the R package **forecast** (Hyndman & Khandakar, 2008).

We define the relative width as the ratio between the width of the reconciled prediction interval and that of the base forecast. In Fig. 3, we show the distribution of the relative width of the 95% prediction intervals of *MinT* and *t-Rec*. The prediction intervals of *MinT* are always narrower than those of the base forecasts; indeed, the relative width is upper-bounded by 1. On the other hand, the relative width of *t-Rec* can be also above one, and it is correlated to the incoherence of the base forecasts.

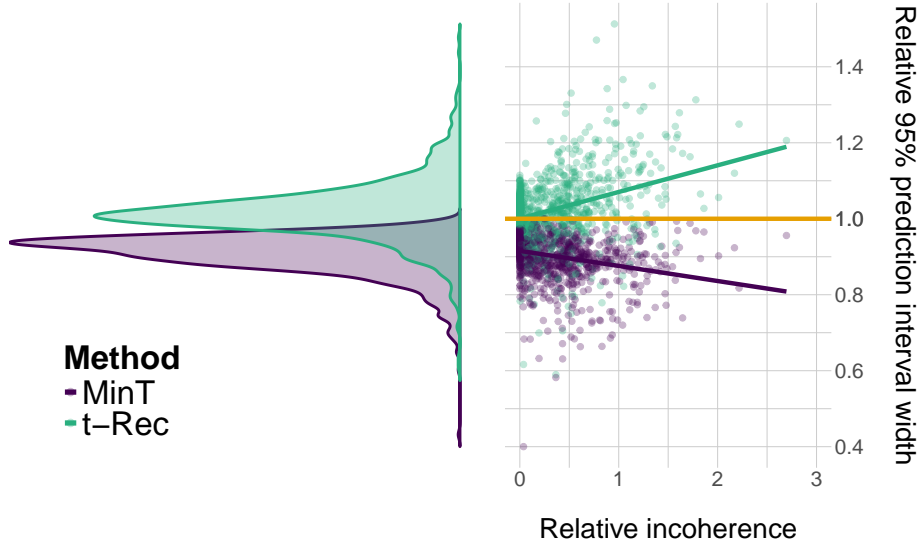


Figure 3: Distributions of the 95% prediction interval widths for *MinT* (purple) and *t-Rec* (green) across 1000 simulations for the upper variable (left panel). Relative 95% predictive interval widths compared to the *Base* method plotted against relative incoherence levels (normalized by the *Base* standard deviation) across 1000 simulations for the upper variable (right panel). *MinT* consistently narrows intervals, while *t-Rec* either widens or narrows them depending on the incoherence level. Notably, *t-Rec* exhibits an increasing trend, with interval widths expanding as incoherence grows.

In Table 1 we report the geometric mean, over the simulations, of the relative width of the prediction intervals for *MinT* and *t-Rec*, for 80% and 95% intervals. For *MinT*, the relative width is less or equal to 1 and remains constant across confidence levels, as it only depends on the ratio of standard deviations between the reconciled and base forecasts. In contrast, the relative width of *t-Rec* varies with the confidence level. Due to the heavier tails of the t-distribution compared to the Gaussian, *t-Rec* has higher relative width at the 95% level than at the 80%.

Relative width of the prediction intervals				
	80%		95%	
	<i>MinT</i>	<i>t-Rec</i>	<i>MinT</i>	<i>t-Rec</i>
U	0.90	0.99	0.90	1.02
B1	0.95	1.01	0.95	1.05
B2	0.95	1.01	0.95	1.05

Table 1: Geometric average over 1000 experiments of the relative width of 80% and 95% predictive intervals, computed with respect to *Base*. A value smaller than 1 implies that on average reconciliation shortens the prediction intervals.

In Fig. 4, we compare the *MinT* and *t-Rec* forecast distributions of the upper-level series for two different simulation runs. We also include the densities of the base forecast distribution and the bottom-up distribution, defined as $\pi_{BU} = \text{MVN}(\widehat{\mathbf{Ab}}, \widehat{\mathbf{A}\Sigma_B\mathbf{A}^T})$. When the incoherence is low (left panel), the reconciled distributions of *MinT* and *t-Rec* are nearly identical. In contrast, when the incoherence is large (right panel), the distribution of *t-Rec* has heavier tails than that of *MinT*.

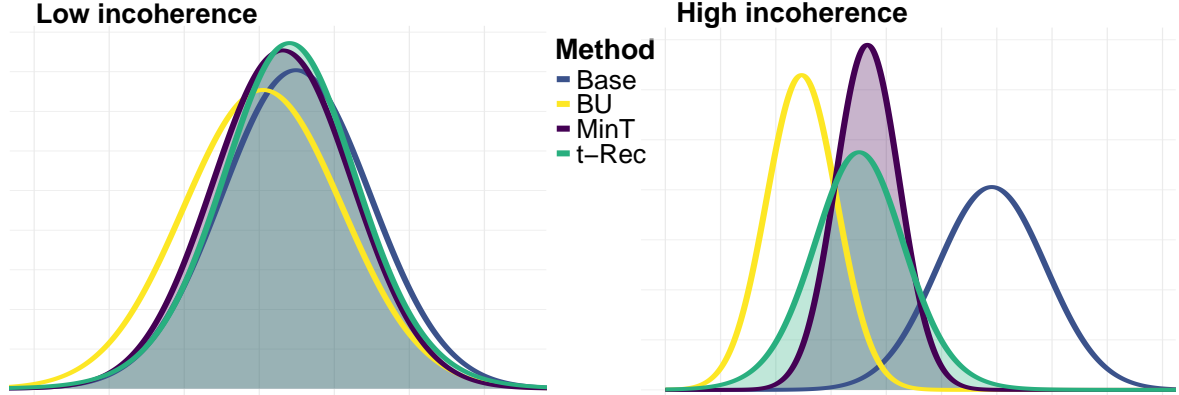


Figure 4: Comparison of predictive densities for the upper time series of the minimal hierarchy. A simulation with little incoherence, where the densities mostly overlap (left); a simulation with large incoherence, where t -Rec has heavier tails than $MinT$ (right).

5. Experiments on real data sets

We evaluate the performance of t -Rec and $MinT$ on three real-world data sets. The first is a novel dataset that we introduce and refer to as *Swiss tourism*, while the other two are established Australian tourism datasets commonly used in the literature.

Swiss tourism. Switzerland consists of 26 cantons, listed in Table 2.

Abbr.	Canton	Abbr.	Canton	Abbr.	Canton
AG	Aargau	NW	Nidwalden	AI	Appenzell Innerrhoden
OW	Obwalden	AR	Appenzell Ausserrhoden	SG	St. Gallen
BE	Bern	SH	Schaffhausen	SO	Solothurn
BL	Basel-Landschaft	BS	Basel-Stadt	FR	Fribourg
GE	Geneva	GL	Glarus	GR	Graubünden
JU	Jura	LU	Lucerne	NE	Neuchâtel
SZ	Schwyz	TG	Thurgau	TI	Ticino
UR	Uri	VD	Vaud	VS	Valais
ZG	Zug	ZH	Zurich		

Table 2: List of the 26 Swiss cantons

We collected monthly records of overnight stays from the Swiss Federal Statistical Office website ¹. The data are originally disaggregated by both canton and country of origin of the tourists. However, for our analysis, we focus solely on the disaggregation by canton. This choice avoids issues with intermittency and sparsity, which occur in more highly disaggregated series and would invalidate the Gaussian residual assumption used in our models.

The resulting hierarchy consists of 26 bottom-level series (one for each canton) and one top-level series (national total). The data comprises 241 monthly observations, from January 2005 to January 2025.

Australian tourism. The other two datasets (*Australian Tourism-M* and *Australian Tourism-Q*) refer to Australian domestic overnight trips ².

Australian Tourism-M dataset is derived from the file *TourismData_v3.csv*, available on Robert Hyndman website ³. It consists of monthly time series structured into a three-level hierarchy. The bottom level includes 76 series representing Australian regions, which are then aggregated into 27 zones, 7 states, and the total.

¹<https://www.pxweb.bfs.admin.ch/pxweb/en/>

²<https://www.tra.gov.au/>

³<https://robjhyndman.com/data/>

This dataset spans from January 1998 to December 2016, covering 228 time points. For a detailed breakdown of this geographical hierarchy, we refer to Table 6 in Wickramasuriya et al. (2019).

We obtain *Australian Tourism-Q* from the `tsibble` R package (Wang, Cook & Hyndman, 2020). It contains quarterly data; it follows a two-level hierarchy, similar to the previous dataset but without the zone level. This dataset covers 20 years, from January 1998 to December 2017, for a total of 80 observations. The main features of all datasets are summarized in Table 3.

Dataset	Frequency	Levels	n_b	n_u	n	Length
Swiss Tourism	Monthly	1	26	1	27	240
Australian Tourism-M	Monthly	3	76	35	111	228
Australian Tourism-Q	Quarterly	2	76	8	84	80

Table 3: Summary of the datasets used in the paper.

Experimental setting. We compute the base forecasts for each time series using the ets model from the `forecast` R package Hyndman & Khandakar (2008). We only consider ets models with additive noise since our model assumes the predictive distribution of the base forecasts to be Gaussian. We compare the base forecasts with the forecast reconciled by *t-Rec* and *MinT*.

We consider different training set lengths; for each length we perform repeated experiments with a rolling origin. We use 100 rolling origins for the monthly data set. With *Australian Tourism-Q*, which has less observation, we use as many rolling origins as possible, depending on the training set length.

Evaluation metrics. We assess the point forecasts through the Mean Squared Error (MSE), averaged over the rolling origins:

$$MSE = \frac{1}{R} \sum_{i=1}^R \|\tilde{\mathbf{y}}_i - \mathbf{y}_i\|_2^2,$$

where $\|\cdot\|_2$ is the Euclidean distance, R is the number of rolling windows, $\tilde{\mathbf{y}}_i \in \mathbb{R}^n$ is the vector of the point forecasts for the i -th rolling window, and $\mathbf{y}_i \in \mathbb{R}^n$ is the vector of the corresponding actual values. We eventually report the relative MSE, i.e., the ratio between the MSE of the reconciled and the base forecasts:

$$RelMSE = \frac{MSE}{MSE_{Base}}. \quad (16)$$

For each series j , with $j = 1, \dots, n$, we assess the predictive distribution using the Continuous Ranked Probability Score (CRPS) (Gneiting & Raftery, 2007):

$$CRPS_j = \frac{1}{R} \sum_{i=1}^R \int_{-\infty}^{+\infty} (F_{i,j}(x) - \mathbb{I}(x \geq y_{i,j}))^2 dx$$

where $F_{i,j}$ is the predictive CDF for the i -th rolling origin and series j and $y_{i,j}$ is the corresponding actual value. We compute the CRPS for both the Gaussian and t distributions in closed form using the `scoringRules` R package (Jordan, Krüger & Lerch, 2019). We score the prediction intervals using the Mean Interval Score (MIS) (Gneiting & Raftery, 2007):

$$MIS_j = \frac{1}{R} \sum_{i=1}^R ((u_{i,j}^\alpha - l_{i,j}^\alpha) + \frac{2}{\alpha} [(l_{i,j}^\alpha - y_{i,j})\mathbb{I}(y_{i,j} < l_{i,j}^\alpha) + (y_{i,j} - u_{i,j}^\alpha)\mathbb{I}(y_{i,j} > u_{i,j}^\alpha)])$$

where $l_{i,j}^\alpha$ and $u_{i,j}^\alpha$ are the lower and upper bounds of the α -level prediction interval for the i -th rolling origin and series j , and $y_{i,j}$ is the corresponding actual value. We consider the 80% and 95% prediction intervals. The CRPS and MIS are univariate scale-dependent scoring rules; we follow the approach of Girolimetto et al. (2024) to aggregate the n scores into a single value by computing the geometric mean of the relative scores with respect to the base forecast:

$$RelCRPS = \left(\prod_{j=1}^n \frac{CRPS_j}{CRPS_{j,Base}} \right)^{\frac{1}{n}}, \quad (17)$$

and we do the same with the relative MIS scores for the 80% and 95% prediction intervals. Finally, we apply the non-parametric Friedman test with Nemenyi post hoc to check the significance of the differences, using the `tsutils` R package (Kourentzes, 2023).

5.1. Swiss Tourism results

We consider training lengths from 30 (two and a half years) to 60 (five years); the results are shown in Fig. 5 as a function of the training set length.

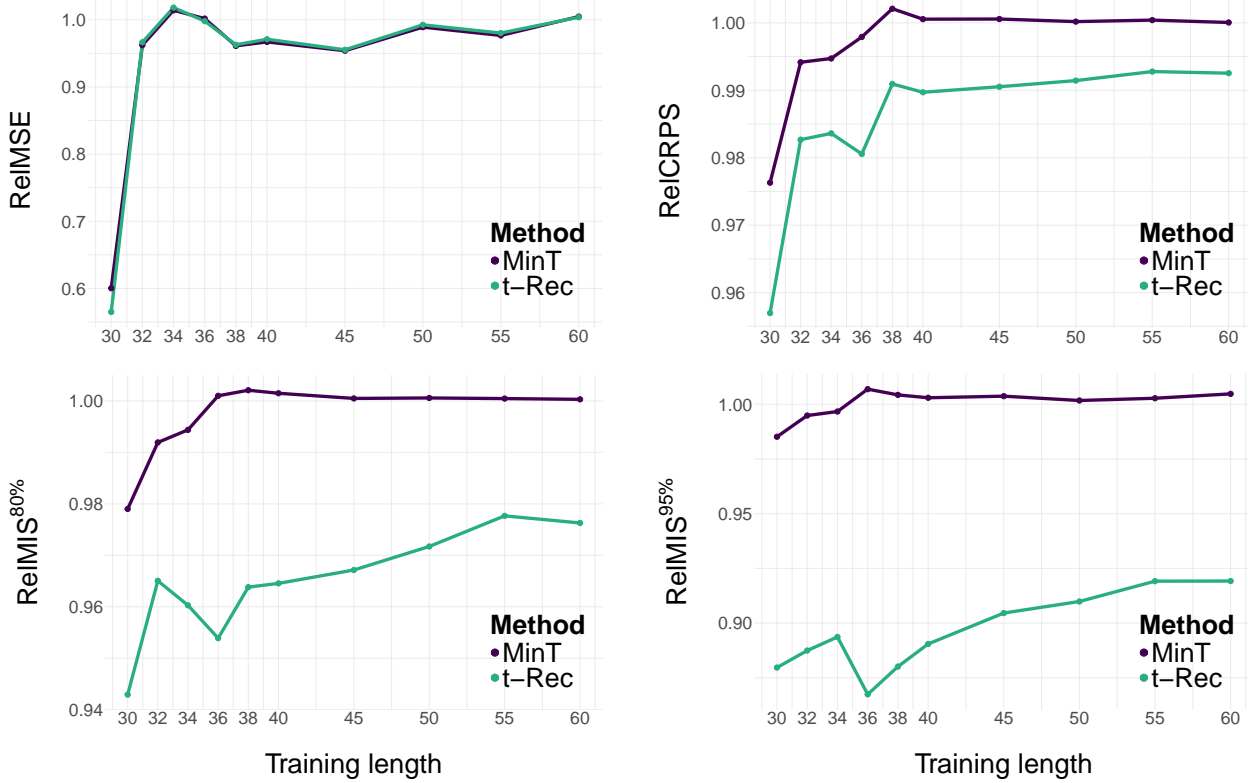


Figure 5: Results on the *Swiss Tourism* dataset for *MinT* (purple) and *t-Rec* (green). A relative score lower than 1 means improvement over the base forecasts.

On MSE the performance of *t-Rec* and *MinT* is very close (top-left plot) at each training length. *t-Rec* has instead an advantage on CRPS and especially on MIS^{80%} and MIS^{95%}. Indeed, the CRPS average the quantile loss over all quantiles, while *t-Rec* especially improves the tails of the predictive distributions. Indeed, *t-Rec* outperforms *MinT* on the MIS, with an especially large advantage for larger confidence levels. This is the effect of the t-distribution's polynomial tails, which allocate more probability mass to the extremes compared to the exponential tails of the Gaussian distribution used in *MinT*. Moreover, *t-Rec* provides better coverage than *MinT* (Fig. 6).

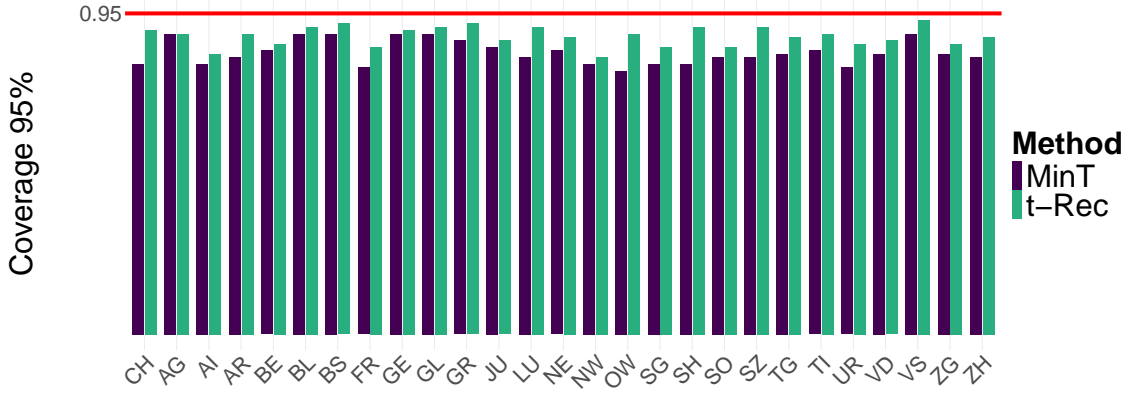


Figure 6: Coverage of the 95% predictive intervals across 100 rolling windows (training length = 40). On every canton, *t*-*Rec* achieves coverage closer to the target (red line) than *MinT*.

Fig. 7 shows the graphs of the Friedman test selecting a training set length of 40 observations.

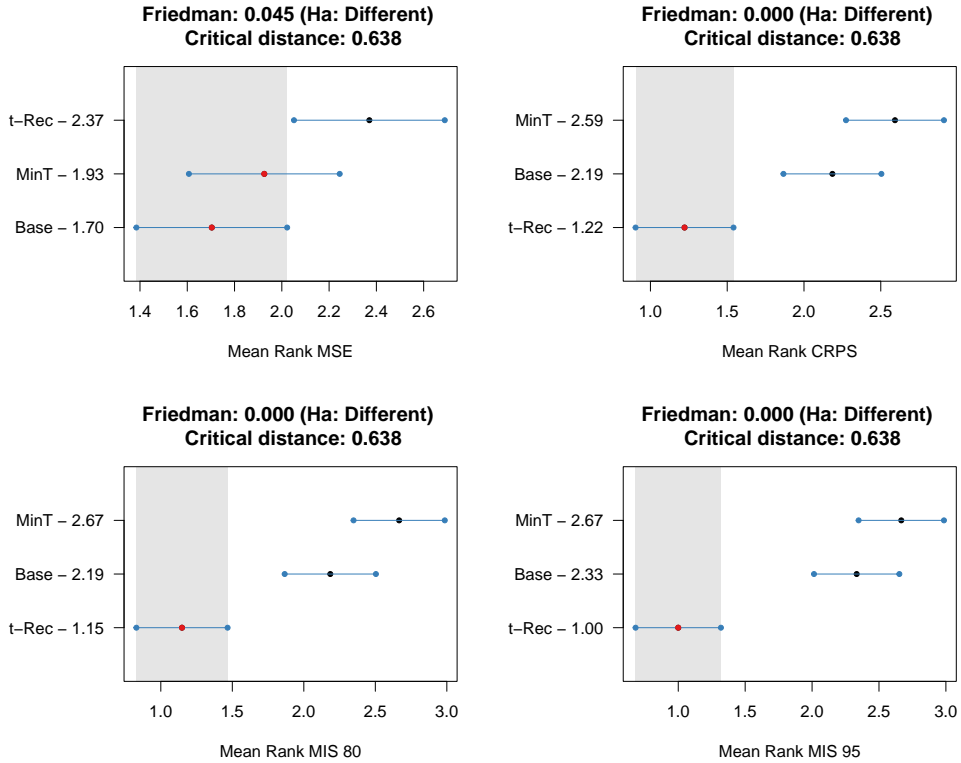


Figure 7: MCB test results for training set length of 40 in the *Swiss Tourism* dataset. The first row shows the MSE and the CRPS, the second row presents the MIS calculated for the 80% and for the 95% predictive intervals.

Fig.8 reports the RelMIS for the 95% prediction intervals at the canton level for a training set length of 40 observations. These results further confirm the superiority of *t*-*Rec* in calibrating prediction intervals across all bottom-level time series. In contrast, *MinT* performs worse than the *Base* method in some cantons, and even when it does improve upon the *Base*, the gains are modest compared to those achieved by *t*-*Rec*. This result justifies the broader predictive interval widths observed in Fig.9, as they allow the method to capture the actual value more frequently. It also suggests that the uncertainty structure among the time

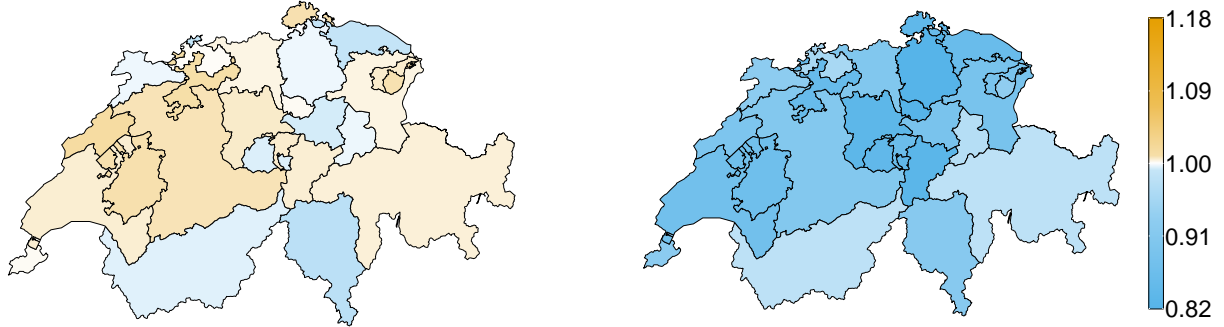


Figure 8: Relative MIS^{95%} in the *Swiss Tourism* dataset, with a training length of 40 observations, shown by canton. The left map displays *MinT*, and the right shows *t-Rec*. Orange-colored cantons indicate worse performance than the *Base* (ratio > 1). *t-Rec* consistently improves MIS^{95%} across all cantons and achieves greater absolute gains than *MinT*.

series is adequately accounted for, as the method produces more robust results.

Moreover, Fig. 9 illustrates how the 95% prediction interval width, both for the upper-level series (left panel) and the geometric mean across bottom-level series (right panel), varies with the incoherence in this real-world setting. A clear positive correlation emerges between the interval widths produced by *t-Rec* and the level of incoherence across all rolling origins. In contrast, *MinT* shows no such dependence.

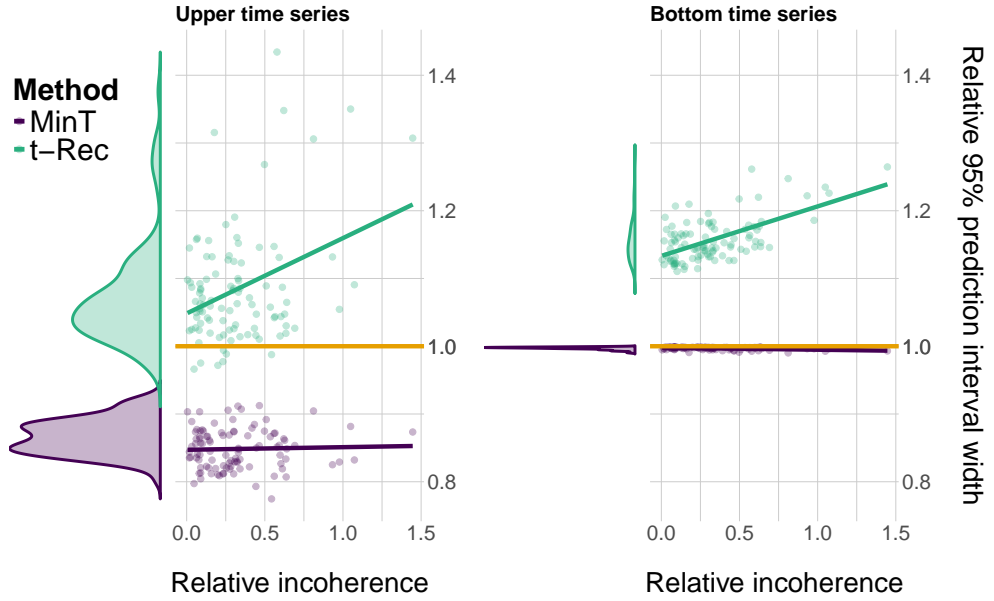


Figure 9: Distributions of 95% prediction interval widths and their relative changes compared to the *Base* method for the *Swiss tourism* dataset. The left panel displays results for the upper-level series, showing the distribution of interval widths for *MinT* (purple) and *t-Rec* (green) across 100 rolling windows, and a scatterplot of relative interval widths versus relative incoherence (normalized by the *Base* standard deviation) across the same windows. The right panel presents the same quantities for the geometric mean over the bottom-level series. In both cases, *MinT* consistently narrows intervals, while *t-Rec* either widens or narrows them depending on the incoherence level. Notably, *t-Rec* exhibits an increasing trend, with interval widths expanding as incoherence grows.

These findings support the value of incorporating covariance matrix uncertainty, as done in *t-Rec*, to better capture the full spectrum of predictive uncertainty. The method proves beneficial even in more challenging reconciliation settings, such as when forecast incoherence is substantial.

5.2. Australian Tourism results

On both *Australian tourism-M* and *Australian tourism-Q* datasets, the performance of *t-Rec* and *MinT* is equivalent on MSE. *t-Rec* has a slight advantage on CRPS and a large advantage on MIS^{80%} and MIS^{95%} (Fig. 10).

These are the same patterns observed in the previous experiments.

As with the *Swiss Tourism* dataset, we report the results on predictive interval width and coverage in Table 4 for two training lengths. We further aggregate the results across series by computing the geometric mean of the predictive interval widths and the arithmetic mean of the coverage rates. Once again, the *t-Rec* method demonstrates improved coverage and more effective interval calibration compared to *MinT*, confirming its robustness across different temporal granularities. By adaptively adjusting interval widths, *t-Rec* consistently achieves superior coverage, underscoring its enhanced ability to model the underlying covariance structure.

		Australian Tourism - M				Australian Tourism - Q			
		Train 55		Train 110		Train 25		Train 40	
Level		<i>MinT</i>	<i>t-Rec</i>	<i>MinT</i>	<i>t-Rec</i>	<i>MinT</i>	<i>t-Rec</i>	<i>MinT</i>	<i>t-Rec</i>
PI Width	80%	0.87	0.92	0.91	0.94	0.95	1.09	0.96	1.12
	95%	0.87	0.93	0.91	0.94	0.95	1.11	0.96	1.13
Coverage	80%	0.73	0.76	0.78	0.80	0.69	0.76	0.69	0.77
	95%	0.88	0.90	0.91	0.92	0.86	0.92	0.87	0.93

Table 4: Predictive interval (PI) width and coverage at the 80% and 95% confidence level for the *Australian Tourism-Q* and *Australian Tourism-M* datasets. Results are reported for various training set lengths.

6. Conclusion

t-Rec performs probabilistic reconciliation accounting for the uncertainty on the covariance matrix. We obtain in closed-form a multivariate-t predictive reconciled distribution. Empirical results show that *t-Rec* consistently outperforms *MinT* on the prediction intervals, while maintaining comparable accuracy in point forecasts. These gains persist even when the number of observations is limited relative to the number of series, and are robust across different training lengths.

Although our analysis focuses on the cross-sectional hierarchical setting, extending the model to the temporal case is straightforward. The main requirement is to define the prior scale matrix in accordance with the temporal hierarchical structure.

From a theoretical perspective, we show that the reconciled variance under *t-Rec* depends explicitly on the level of incoherence in the forecasts. This dependence is confirmed empirically, suggesting that incorporating prior information into the reconciliation process can lead to more reliable uncertainty quantification.

However, we acknowledge the limitations of the IW prior, particularly in high-dimensional settings (Gelman, 2006). Future work will explore more flexible priors for covariance matrices and assess their impact on reconciliation performance.

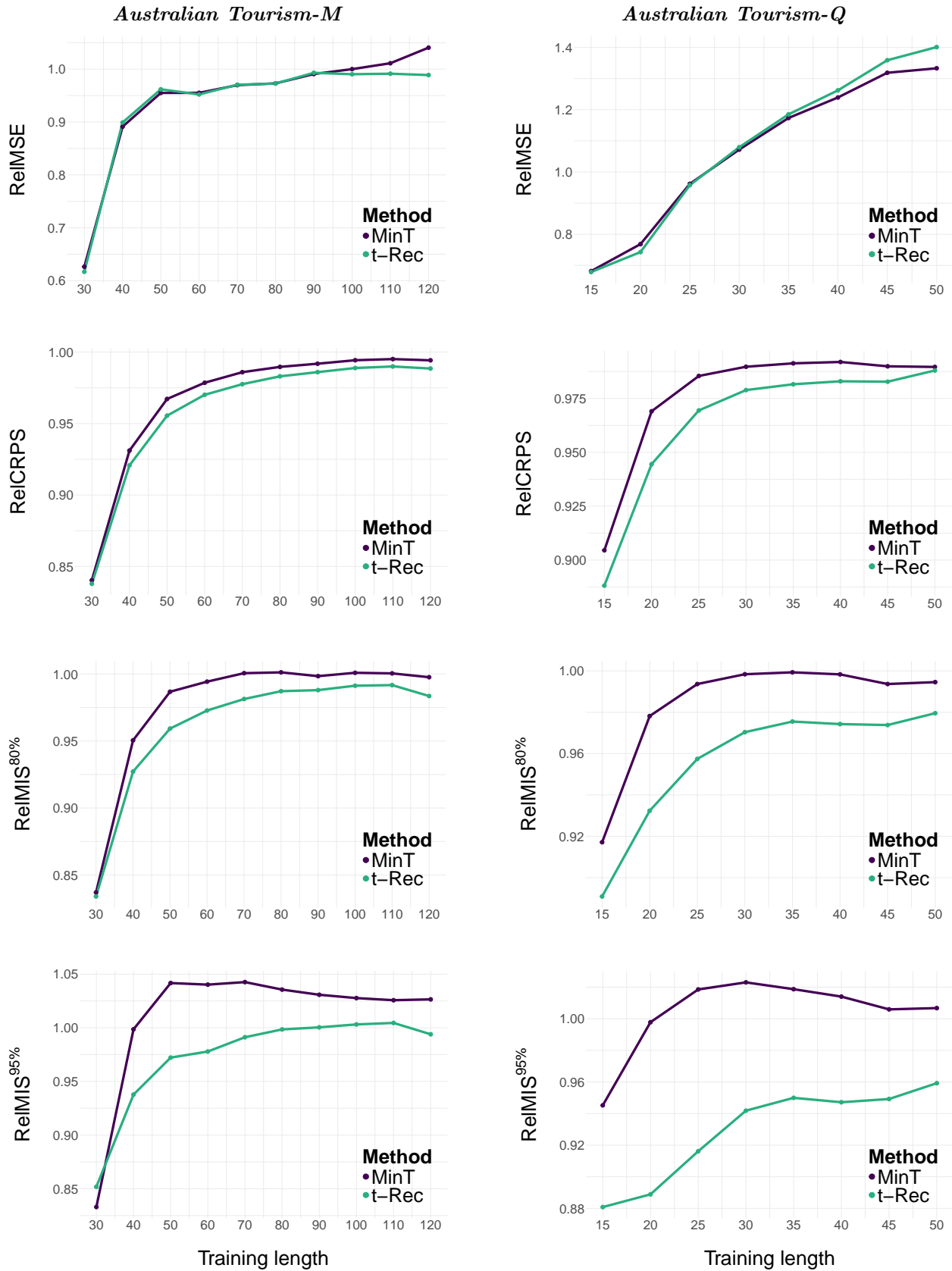


Figure 10: Results on the *Australian Tourism-M* (left column) and *Australian Tourism-Q* (right column) datasets for *MinT* (purple) and *t-Rec* (green). A relative score lower than 1 means improvement over the base forecasts.

References

Carrara, C., Zambon, L., Azzimonti, D., & Corani, G. (2025). A novel shrinkage estimator of the covariance matrix for hierarchical time series. In E. di Bella, V. Gioia, C. Lagazio, & S. Zaccarin (Eds.), *Statistics for Innovation I* (pp. 140–145). Cham: Springer Nature Switzerland.

Corani, G., Azzimonti, D., Augusto, J. P., & Zaffalon, M. (2020). Probabilistic Reconciliation of Hierarchical Forecast via Bayes' Rule. In *Proc. European Conf. On Machine Learning and Knowledge Discovery in Database ECML/PKDD* (pp. 211–226). volume 3.

Di Fonzo, T., & Girolimetto, D. (2024). Forecast combination-based forecast reconciliation: Insights and extensions. *International Journal of Forecasting*, 40, 490–514.

Gelman, A. (2006). Prior distributions for variance parameters in hierarchical models (Comment on Article by Browne and Draper). *Bayesian Analysis*, 1, 515–534.

Gelman, A., Carlin, J., Stern, H., Dunson, D., Vehtari, A., & Rubin, D. (2013). *Bayesian Data Analysis* (3rd ed.). Chapman and Hall/CRC.

Girolimetto, D., Athanasopoulos, G., Di Fonzo, T., & Hyndman, R. J. (2024). Cross-temporal probabilistic forecast reconciliation: Methodological and practical issues. *International Journal of Forecasting*, 40, 1134–1151.

Girolimetto, D., & Fonzo, T. D. (2024). Point and probabilistic forecast reconciliation for general linearly constrained multiple time series. *Statistical Methods & Applications*, 33, 581–607. URL: <https://doi.org/10.1007/s10260-023-00738-6>. doi:10.1007/s10260-023-00738-6.

Gneiting, T., & Raftery, A. E. (2007). Strictly proper scoring rules, prediction, and estimation. *Journal of the American statistical Association*, 102, 359–378.

Gupta, A. K., & Nagar, D. K. (2018). *Matrix variate distributions*. Chapman and Hall/CRC.

Hollyman, R., Petropoulos, F., & Tipping, M. E. (2021). Understanding forecast reconciliation. *European Journal of Operational Research*, 294, 149–160.

Hyndman, R. J., & Khandakar, Y. (2008). Automatic time series forecasting: the forecast package for R. *Journal of statistical software*, 27, 1–22.

Johnson, S. G. (2008). *The NLOpt nonlinear-optimization package*. URL: <https://github.com/stevengj/nlopt>.

Jordan, A., Krüger, F., & Lerch, S. (2019). Evaluating Probabilistic Forecasts with scoringRules. *Journal of Statistical Software*, 90, 1–37. doi:10.18637/jss.v090.i12.

Kotz, S., & Nadarajah, S. (2004). *Multivariate T-Distributions and Their Applications*. Cambridge University Press.

Kourentzes, N. (2023). *tsutils: Time Series Exploration, Modelling and Forecasting*. URL: <https://CRAN.R-project.org/package=tsutils> r package version 0.9.4.

Panagiotelis, A., Athanasopoulos, G., Gamakumara, P., & Hyndman, R. J. (2021). Forecast reconciliation: A geometric view with new insights on bias correction. *International Journal of Forecasting*, 37, 343–359.

Panagiotelis, A., Gamakumara, P., Athanasopoulos, G., & Hyndman, R. J. (2023). Probabilistic forecast reconciliation: Properties, evaluation and score optimisation. *European Journal of Operational Research*, 306, 693–706.

Pritularga, K. F., Svetunkov, I., & Kourentzes, N. (2021). Stochastic coherency in forecast reconciliation. *International Journal of Production Economics*, 240, 108221.

Schäfer, J., & Strimmer, K. (2005). A shrinkage approach to large-scale covariance matrix estimation and implications for functional genomics. *Statistical applications in genetics and molecular biology*, 4.

Sherman, J., & Morrison, W. J. (1950). Adjustment of an inverse matrix corresponding to a change in one element of a given matrix. *The Annals of Mathematical Statistics*, 21, 124–127.

Vehtari, A., Gelman, A., & Gabry, J. (2017). Practical Bayesian model evaluation using leave-one-out cross-validation and WAIC. *Statistics and computing*, 27, 1413–1432.

Wang, E., Cook, D., & Hyndman, R. J. (2020). A new tidy data structure to support exploration and modeling of temporal data. *Journal of Computational and graphical Statistics*, 29, 466–478.

Wickramasuriya, S. L. (2017). *Optimal Forecasts for Hierarchical and Grouped Time Series*. Ph.D. thesis Monash University. URL: https://bridges.monash.edu/articles/thesis/Optimal_forecasts_for_hierarchical_and_grouped_time_series/5032136. doi:10.4225/03/5923c4e094308.

Wickramasuriya, S. L. (2024). Probabilistic forecast reconciliation under the Gaussian framework. *Journal of Business & Economic Statistics*, 42, 272–285.

Wickramasuriya, S. L., Athanasopoulos, G., & Hyndman, R. J. (2019). Optimal forecast reconciliation for hierarchical and grouped time series through trace minimization. *Journal of the American Statistical Association*, 114, 804–819.

Yang, Y. F., Athanasopoulos, G., Hyndman, R. J., & Panagiotelis, A. (2024). Forecast Linear Augmented Projection (FLAP): A free lunch to reduce forecast error variance. *arXiv preprint arXiv:2407.01868*, .

Zambon, L., Agosto, A., Giudici, P., & Corani, G. (2024a). Properties of the reconciled distributions for Gaussian and count forecasts. *International Journal of Forecasting*, 40, 1438–1448.

Zambon, L., Azzimonti, D., & Corani, G. (2024b). Efficient probabilistic reconciliation of forecasts for real-valued and count time series. *Statistics and Computing*, 34, 21.

Zambon, L., Azzimonti, D., Rubattu, N., & Corani, G. (2024c). Probabilistic reconciliation of mixed-type hierarchical time series. In *The 40th Conference on Uncertainty in Artificial Intelligence*.

Appendix A. Reconciliation via conditioning of multivariate t

Similarly to the Gaussian case (Zambon et al., 2024a), if the joint base forecast distribution is a multivariate t, then the reconciled distribution and the parameters can be computed in closed-form. Theorem 1 is proved by applying the following result to Eq. (7).

Proposition 1. *Let $\mathbf{A} \in \mathbb{R}^{(n-n_b) \times n_b}$ be the aggregation matrix of a hierarchy with n time series, and let the joint forecast distribution be a multivariate t: $\widehat{\mathbf{Y}} \sim \text{mt}(\widehat{\mathbf{y}}, \widehat{\boldsymbol{\Psi}}, \widehat{\nu})$. Then, the reconciled distribution via conditioning of the n_b bottom series is still a multivariate t:*

$$\widetilde{\mathbf{B}} \sim \text{mt}(\widetilde{\mathbf{b}}, \widetilde{\boldsymbol{\Sigma}}_B, \widetilde{\nu}_B), \quad (\text{A.1})$$

where

$$\widetilde{\mathbf{b}} = \widehat{\mathbf{b}} + \left(\widehat{\boldsymbol{\Psi}}_{UB}^T - \widehat{\boldsymbol{\Psi}}_B \mathbf{A}^T \right) \mathbf{Q}^{-1} (\mathbf{A} \widehat{\mathbf{b}} - \widehat{\mathbf{u}}), \quad (\text{A.2})$$

$$\widetilde{\boldsymbol{\Sigma}}_B = C \left[\widehat{\boldsymbol{\Psi}}_B - \left(\widehat{\boldsymbol{\Psi}}_{UB}^T - \widehat{\boldsymbol{\Psi}}_B \mathbf{A}^T \right) \mathbf{Q}^{-1} \left(\widehat{\boldsymbol{\Psi}}_{UB}^T - \widehat{\boldsymbol{\Psi}}_B \mathbf{A}^T \right)^T \right], \quad (\text{A.3})$$

$$\widetilde{\nu}_B = \widehat{\nu} + n - n_b, \quad (\text{A.4})$$

and

$$\begin{aligned} C &= \frac{\widehat{\nu} + (\mathbf{A} \widehat{\mathbf{b}} - \widehat{\mathbf{u}})^T \mathbf{Q}^{-1} (\mathbf{A} \widehat{\mathbf{b}} - \widehat{\mathbf{u}})}{\widehat{\nu} + (n - n_b)}, \\ \mathbf{Q} &= \widehat{\boldsymbol{\Psi}}_U - \widehat{\boldsymbol{\Psi}}_{UB} \mathbf{A}^T - \mathbf{A} \widehat{\boldsymbol{\Psi}}_{UB}^T + \mathbf{A} \widehat{\boldsymbol{\Psi}}_B \mathbf{A}^T. \end{aligned} \quad (\text{A.5})$$

To prove Proposition 1, we first state two technical lemmas about key properties of the multivariate t distribution. For a proof of these lemmas, we refer to Kotz & Nadarajah (2004).

Lemma 1. *Let \mathbf{X} be a n -dimensional random vector distributed as a multivariate t:*

$$\mathbf{X} \sim \text{mt}(\boldsymbol{\mu}, \boldsymbol{\Sigma}, \nu),$$

and let $\mathbf{V} \in \mathbb{R}^{n \times n}$ be full-rank. Then, the random vector $\mathbf{V}\mathbf{X}$ is distributed as a multivariate t:

$$\mathbf{V}\mathbf{X} \sim \text{mt}(\mathbf{V}\boldsymbol{\mu}, \mathbf{V}\boldsymbol{\Sigma}\mathbf{V}^T, \nu).$$

Lemma 2. *Let $\mathbf{X} = \begin{bmatrix} \mathbf{X}_1 \\ \mathbf{X}_2 \end{bmatrix} \sim \text{mt} \left(\begin{bmatrix} \boldsymbol{\mu}_1 \\ \boldsymbol{\mu}_2 \end{bmatrix}, \begin{bmatrix} \boldsymbol{\Sigma}_{11} & \boldsymbol{\Sigma}_{12} \\ \boldsymbol{\Sigma}_{21} & \boldsymbol{\Sigma}_{22} \end{bmatrix}, \nu \right)$. Then, the conditional distribution of \mathbf{X}_1 given \mathbf{X}_2 is still a multivariate t:*

$$\mathbf{X}_1 | \mathbf{X}_2 \sim \text{mt}(\boldsymbol{\mu}_{1|2}, \boldsymbol{\Sigma}_{1|2}, \nu_{1|2}), \quad (\text{A.6})$$

where

$$\boldsymbol{\mu}_{1|2} = \boldsymbol{\mu}_1 + \boldsymbol{\Sigma}_{12} \boldsymbol{\Sigma}_{22}^{-1} (\mathbf{x}_2 - \boldsymbol{\mu}_2), \quad (\text{A.7})$$

$$\boldsymbol{\Sigma}_{1|2} = \frac{\nu + (\mathbf{x}_2 - \boldsymbol{\mu}_2)^T \boldsymbol{\Sigma}_{22}^{-1} (\mathbf{x}_2 - \boldsymbol{\mu}_2)}{\nu + n_2} \left[\boldsymbol{\Sigma}_{11} - \boldsymbol{\Sigma}_{12} \boldsymbol{\Sigma}_{22}^{-1} \boldsymbol{\Sigma}_{21} \right], \quad (\text{A.8})$$

$$\nu_{1|2} = \nu + n_2. \quad (\text{A.9})$$

Proof of Proposition 1. Let us define $\mathbf{T} \in \mathbb{R}^{n \times n}$ as

$$\mathbf{T} = \begin{bmatrix} \mathbf{0} & \mathbf{I}_{n_b} \\ \mathbf{I}_{n-n_b} & -\mathbf{A} \end{bmatrix},$$

and let $\mathbf{Z} := \mathbf{T}\widehat{\mathbf{Y}}$. Since \mathbf{T} is full-rank, from Lemma 1, \mathbf{Z} is a multivariate t:

$$\mathbf{Z} \sim \text{mt}(\mathbf{T}\widehat{\mathbf{y}}, \mathbf{T}\widehat{\boldsymbol{\Psi}}\mathbf{T}^T, \widehat{\nu}), \quad (\text{A.10})$$

where

$$\begin{aligned}\mathbf{T}\hat{\mathbf{y}} &= \begin{bmatrix} \hat{\mathbf{b}} \\ \hat{\mathbf{u}} - \mathbf{A}\hat{\mathbf{b}} \end{bmatrix}, \\ \mathbf{T}\hat{\Psi}\mathbf{T}^T &= \begin{bmatrix} \hat{\Psi}_B & \hat{\Psi}_{UB}^T - \hat{\Psi}_B\mathbf{A}^T \\ \hat{\Psi}_{UB} - \mathbf{A}\hat{\Psi}_B & \mathbf{Q} \end{bmatrix},\end{aligned}\tag{A.11}$$

and $\mathbf{Q} = \hat{\Psi}_U - \hat{\Psi}_{UB}\mathbf{A}^T - \mathbf{A}\hat{\Psi}_{UB}^T + \mathbf{A}\hat{\Psi}_B\mathbf{A}^T$. Since

$$\mathbf{Z} = \begin{bmatrix} \hat{\mathbf{B}} \\ \hat{\mathbf{U}} - \mathbf{A}\hat{\mathbf{B}} \end{bmatrix} =: \begin{bmatrix} \mathbf{Z}_1 \\ \mathbf{Z}_2 \end{bmatrix},$$

the reconciled bottom distribution is given by the conditional distribution of \mathbf{Z}_1 given $\mathbf{Z}_2 = 0$. From Lemma 2, we have that

$$\mathbf{Z}_1 | \mathbf{Z}_2 = 0 \sim \text{mt}(\boldsymbol{\mu}_{1|2}, \boldsymbol{\Sigma}_{1|2}, \tilde{\nu}_{1|2}),$$

where

$$\begin{aligned}\boldsymbol{\mu}_{1|2} &= \hat{\mathbf{b}} + (\hat{\Psi}_{UB}^T - \hat{\Psi}_B\mathbf{A}^T)\mathbf{Q}^{-1}(\mathbf{A}\hat{\mathbf{b}} - \hat{\mathbf{u}}) = \tilde{\mathbf{b}}, \\ \tilde{\nu}_{1|2} &= \hat{\nu} + (n - n_b) = \tilde{\nu}_B, \\ \boldsymbol{\Sigma}_{1|2} &= \frac{\hat{\nu} + (\mathbf{A}\hat{\mathbf{b}} - \hat{\mathbf{u}})^T\mathbf{Q}^{-1}(\mathbf{A}\hat{\mathbf{b}} - \hat{\mathbf{u}})}{\hat{\nu} + (n - n_b)} \left[\hat{\Psi}_B - (\hat{\Psi}_{UB}^T - \hat{\Psi}_B\mathbf{A}^T)\mathbf{Q}^{-1}(\hat{\Psi}_{UB}^T - \hat{\Psi}_B\mathbf{A}^T)^T \right] \\ &= C \left[\hat{\Psi}_B - (\hat{\Psi}_{UB}^T - \hat{\Psi}_B\mathbf{A}^T)\mathbf{Q}^{-1}(\hat{\Psi}_{UB}^T - \hat{\Psi}_B\mathbf{A}^T)^T \right] = \tilde{\boldsymbol{\Sigma}}_B.\end{aligned}$$

□

Appendix B. Simulation setup

For the experiments in Sect. 4, we adopt a simulation framework similar to that described in Sect. 3.4 of Wickramasuriya et al. (2019). We consider the minimal hierarchy of Fig. 2. The length of the time series is set to 12. The bottom-level time series are simulated using a basic structural time series model defined as:

$$\mathbf{b}_t = \boldsymbol{\mu}_t + \boldsymbol{\gamma}_t + \boldsymbol{\eta}_t,$$

where $\boldsymbol{\mu}_t$ is the trend component, $\boldsymbol{\gamma}_t$ is the seasonal component, and $\boldsymbol{\eta}_t$ is the error component. The trend component evolves according to a local linear trend model:

$$\begin{aligned}\boldsymbol{\mu}_t &= \boldsymbol{\mu}_{t-1} + \boldsymbol{\nu}_t + \boldsymbol{\varepsilon}_t, & \boldsymbol{\varepsilon}_t &\sim \mathcal{N}(0, 2I_2), \\ \boldsymbol{\nu}_t &= \boldsymbol{\nu}_{t-1} + \boldsymbol{\zeta}_t, & \boldsymbol{\zeta}_t &\sim \mathcal{N}(0, 0.007I_2),\end{aligned}$$

where $\boldsymbol{\varepsilon}_t$, $\boldsymbol{\zeta}_t$, and $\boldsymbol{\omega}_t$ are mutually independent and also independent over time. The seasonal component is defined by:

$$\boldsymbol{\gamma}_t = - \sum_{i=1}^{s-1} \boldsymbol{\gamma}_{t-i} + \boldsymbol{\omega}_t, \quad \boldsymbol{\omega}_t \sim \mathcal{N}(0, 7I_2),$$

with the number of seasons per year set to $s = 4$ to reflect quarterly data. The initial states $\boldsymbol{\mu}_0$, $\boldsymbol{\nu}_0$, $\boldsymbol{\gamma}_0$, $\boldsymbol{\gamma}_1$, and $\boldsymbol{\gamma}_2$ are independently drawn from a multivariate normal distribution with mean zero and identity covariance matrix. The error component $\boldsymbol{\eta}_t$ for each series is generated from an ARIMA(1, 0, 1) model with $\phi_1 = 0.3$ and $\theta_1 = 0.5$; we use $\begin{bmatrix} 5 & 3 \\ 3 & 4 \end{bmatrix}$ as contemporaneous error covariance matrix, the same of series AA and AB in Wickramasuriya et al. (2019). Finally, the upper level series is obtained by summing the bottom-level series.

Appendix C. Diagonal prior

We compare the performance of $MinT$ and the model presented in Sec.3 with two different prior specifications, on the *Swiss Tourism* dataset presented in Sec. 5.1. The first prior is based on a shrinkage estimator of the full covariance matrix of residuals from naive or seasonal naive forecasts and is the one used in t -*Rec*. The second prior uses only the diagonal of the same matrix, thus ignoring residual correlations.

As shown in Fig. C.11, the model with the diagonal prior already outperforms $MinT$, demonstrating the benefit of incorporating parameter uncertainty. However, using the full covariance matrix as prior information leads to even better results, highlighting the additional performance gains achievable by leveraging correlation structure among residuals.

For this reason, we propose t -*Rec* as the central reconciliation method of this paper.

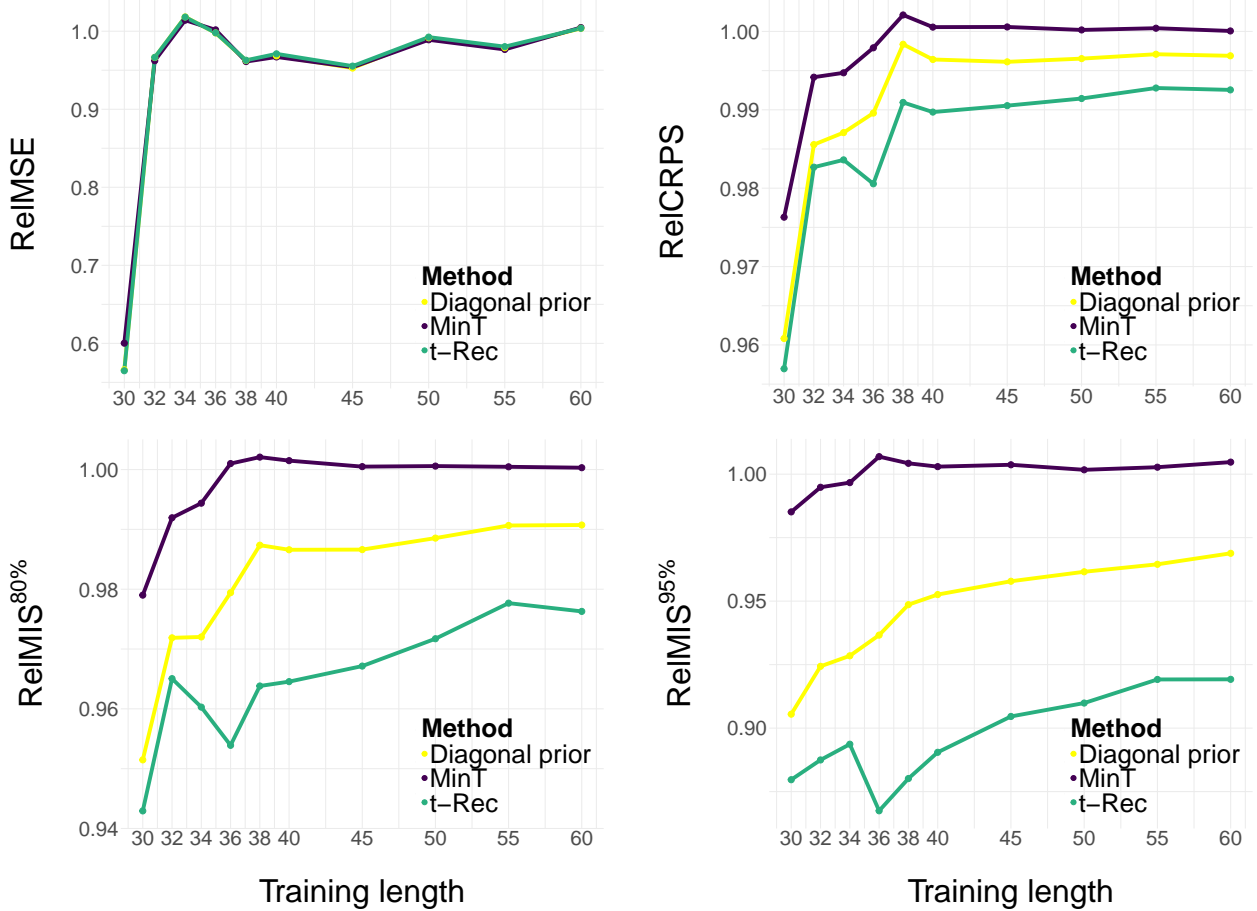


Figure C.11: Results on the *Swiss Tourism* dataset for $MinT$ (purple), proposed model with full covariance matrix as prior t -*Rec* (green) and proposed model with diagonal covariance matrix as prior (yellow). A relative score lower than 1 means improvement over the base forecasts.

Appendix D. Significance results - Australian tourism

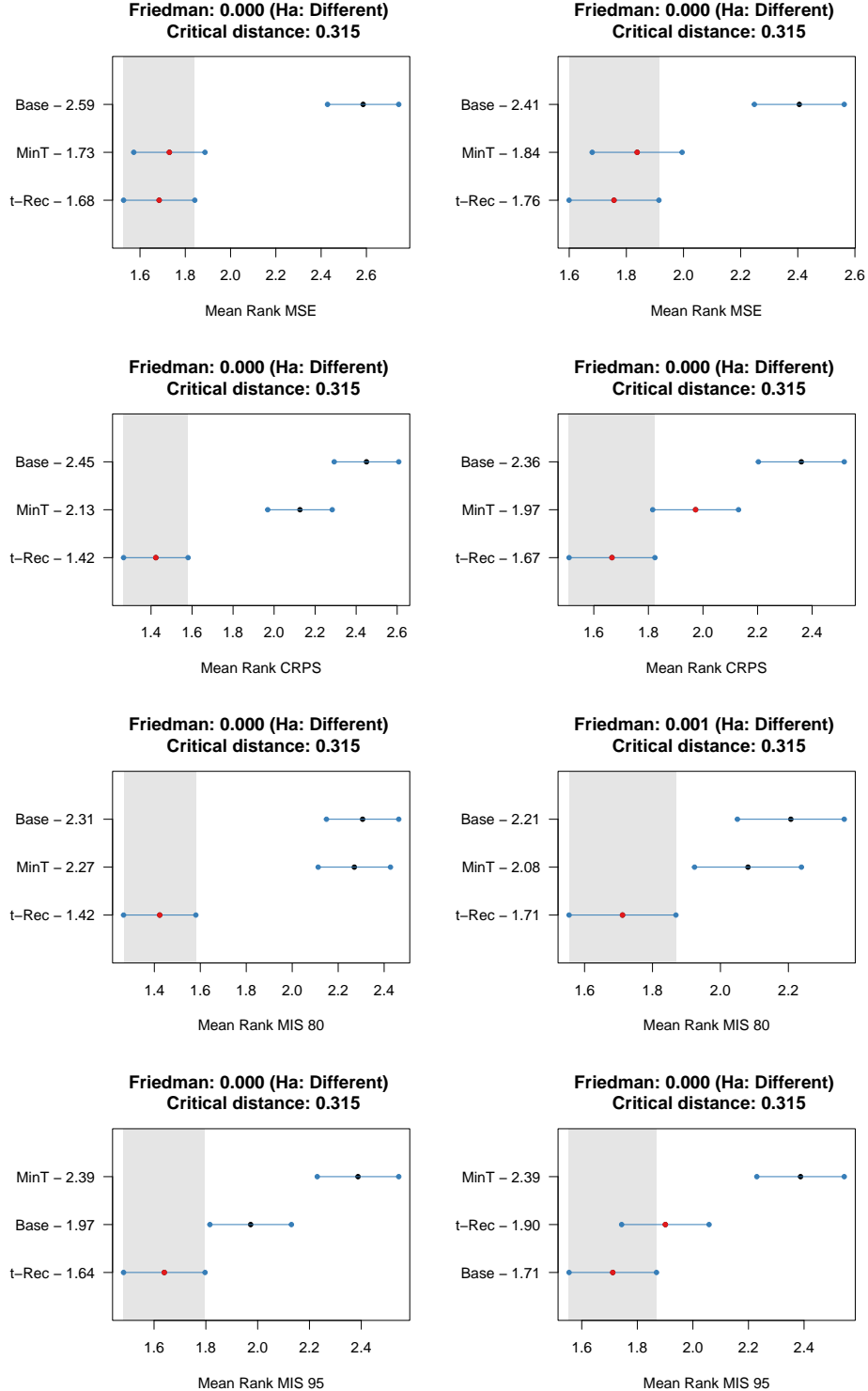


Figure D.12: MCB test results for the *Australian tourism-M* dataset. The columns represent different choices of training length: 55 and 110 observations, respectively. The rows correspond to the metrics: the first row shows the MSE, the second row displays the CRPS, the third row presents the MIS calculated for the 80% predictive interval, and the fourth the MIS calculated for the 95% predictive interval.

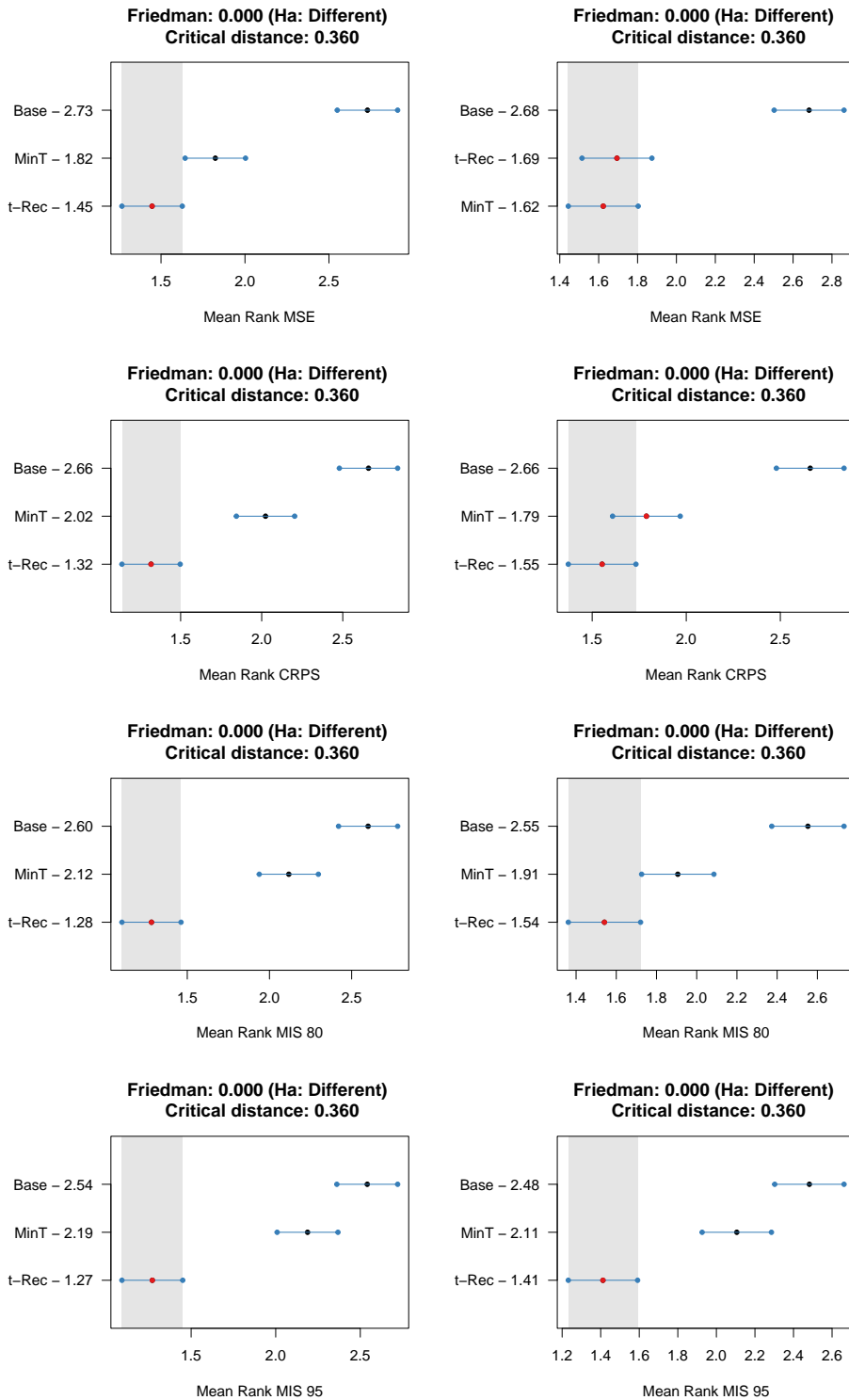


Figure D.13: MCB test results for the *Australian tourism-Q* dataset. The columns represent different choices of training length: 25 and 40 observations, respectively. The rows correspond to the metrics: the first row shows the MSE, the second row displays the CRPS, the third row presents the MIS calculated for the 80% predictive interval, and the fourth the MIS calculated for the 95% predictive interval.